Radiology

Validation of Computational Fluid Dynamics in CT-based Airway Models with SPECT/CT[1]

Jan W. De Backer, MSc, PhD
Wim G. Vos, MSc
Samir C. Vinchurkar, MSc, PhD
Rita Claes
Anton Drollmann, MD
Denis Wulfrank, MD, PhD
Paul M. Parizel, MD, PhD
Paul Germonpré, MD, PhD
Wilfried De Backer, MD, PhD

Purpose: To compare the results obtained by using numerical flow simulations with the results of combined single photon emission computed tomography (SPECT) and computed tomography (CT) and to demonstrate the importance of correct boundary conditions for the numerical methods to account for the large amount of interpatient variability in airway geometry.

Materials and Methods: This study was approved by all relevant institutional review boards. All patients gave their signed informed consent. In this study, six patients with mild asthma (three men; three women; overall mean age, 46 years ± 17 [standard deviation]) underwent CT at functional residual capacity and total lung capacity, as well as SPECT/CT. CT data were used for segmentation and computational fluid dynamics (CFD) simulations. A comparison was made between airflow distribution, as derived with *(a)* SPECT/CT through tracer concentration analysis, *(b)* CT through lobar expansion measurement, and *(c)* CFD through flow computer simulation. Also, the heterogeneity of the ventilation was examined.

Results: Good agreement was found between SPECT/CT, CT, and CFD in terms of airflow distribution and hot spot detection. The average difference for the internal airflow distribution was less than 3% for CFD and CT versus SPECT/CT. Heterogeneity in ventilation patterns could be detected with SPECT/CT and CFD.

Conclusion: This results of this study show that patient-specific computer simulations with appropriate boundary conditions yield information that is similar to that obtained with functional imaging tools, such as SPECT/CT.

Supplemental material: *http://radiology.rsna.org/lookup/suppl/doi:10.1148/radiol.10100322/-/DC1*

[1] From FluidDA, Groeningenlei 132, 2550 Kontich, Belgium (J.W.D.B., W.G.V., S.C.V.); Departments of Respiratory Medicine (R.C., P.G., W.D.B.) and Radiology (P.M.P.), University Hospital Antwerp, Antwerp, Belgium; Novartis, Basel, Switzerland (A.D.); and Department of Nuclear Medicine, AZ Maria Middelares, Ghent, Belgium (D.W.). Received February 9, 2010; revision requested April 2; revision received June 21; accepted July 28; final version accepted August 18. Supported by Novartis. **Address correspondence to** J.W.D.B. (e-mail: *Jan.DeBacker@FluidDA.com*).

The high image resolution and short exposure time (2–8 sec) of thin-section computed tomography (CT) of the thorax have made this modality useful in the assessment of airway structure (1). This modality has greatly increased understanding of the pathophysiology of respiratory diseases, such as chronic obstructive pulmonary disease (2–4), asthma (5–7), and cystic fibrosis (8–10). Furthermore, imaging complements respiratory tests, such as spirometry and body plethysmography, that describe the function of the respiratory system predominantly as a black box, without providing regional information.

In recent studies, the static images obtained with CT have been made more functional by means of computational fluid dynamics (CFD) (11–13). With this method, numerical flow equations (Navier-Stokes equations) are solved on a computational grid (14). This implies that a computer model must be made from the flow domain. Previous articles have stressed the importance of using patient-specific models and boundary conditions (15). In the respiratory field, patient-specific models are obtained via segmentation of the airway structure based on CT and magnetic resonance images. The result of a CFD computation is a description of flow characteristics, such as pressure and velocities through the entire respiratory model. In addition, by solving the force-mass balance on injected discrete particles, it is possible to determine the fates and deposition patterns of inhaled aerosols (16–18).

In clinical practice, the distribution of ventilation in the airways and lungs of a patient is determined with two-dimensional gamma scintigraphy (19,20) or a more advanced technique, such as three-dimensional combined single photon emission CT (SPECT) and CT (21,22,23).

Gases or radiolabeled aerosols can be used for ventilation studies. Deposition of the aerosol particles after inhalation depends on the aerodynamic properties of the particles (mainly their size) and the patient characteristics. In addition, factors affecting global and regional aerosol absorption may also affect pulmonary biodistribution. For alveolar deposition, droplet size should not exceed 2 μm. Larger particles may deposit in the upper airways, leading to hot spots. However, in patients with severe obstructive airway disease, even small particles may deposit in turbulent flow at stenoses. Breathing pattern is also important; at slow tidal breathing, even relatively large particles may reach the lung periphery. In clinical practice in Europe, the most commonly used radioaerosol is technetium 99m (^{99m}Tc) pentetic acid. Several nebulizers for ^{99m}Tc pentetic acid are available on the market. With ^{99m}Tc pentetic acid (SmartVent; Diagnostic Imaging, Welford, England), the average particle size is 1.32 μm. In patients who do not have severe airway stenoses and who are performing slow tidal breathing, adequate homogeneity in ventilation can be achieved.

After inhalation of the radiolabeled aerosol, the distribution of this tracer in the lungs is assessed on either two-dimensional planar projections acquired with two-dimensional gamma scintigraphy or three-dimensional axial sections acquired with SPECT. If the SPECT image is combined with a low-dose CT image, it is possible to fuse both images to obtain a clear indication of the location of certain tracer features, such as hot spots or poorly ventilated areas. In some studies, researchers used SPECT to assess differences in lung ventilation between different types of patients, such as smokers, nonsmokers, and those with emphysema (24,25). The authors concluded that SPECT after radiolabeled aerosol inhalation was a valuable tool with which to describe lung ventilation.

To expand the use of CFD in the respiratory field, it is necessary to validate the outcome of the models with clinical data. In previous studies, researchers have extensively compared CFD data with the outcome of experimental and in vitro setups (26,27). They generally concluded that good agreement could be found when one used similar boundary conditions for both the computational model and the experimental setup. In other studies, researchers compared CFD-based flow characteristics with clinical tests, such as two-dimensional gamma scintigraphy, where it was demonstrated that the results were well within the accuracy limits of the clinical tests (28). However, few studies have compared fused SPECT/CT images with CFD in patients with asthma.

Thus, the aim of this study was to compare the results obtained by using

Advances in Knowledge

- Functional imaging methods that use a combination of CT and patient-specific computer simulations yield results that agree well with SPECT/CT results, with an average difference of less than 3%.
- With this approach, it is possible to obtain insight into the patient-specific airflow patterns in the lower airways.
- This method can be used in future studies to determine regional lung ventilation and airway recruitment in a clinical setting and to potentially optimize inhalation treatment.

Implication for Patient Care

- These methods enable a detailed analysis of the respiratory system, with patient involvement limited to two CT examinations.

Published online
10.1148/radiol.10100322

Radiology 2010; 257:854–862

Abbreviations:
CFD = computational fluid dynamics
FRC = functional residual capacity
TLC = total lung capacity

Author contributions:
Guarantors of integrity of entire study, J.W.D.B., S.C.V., R.C., W.D.B.; study concepts/study design or data acquisition or data analysis/interpretation, all authors; manuscript drafting or manuscript revision for important intellectual content, all authors; manuscript final version approval, all authors; literature research, J.W.D.B., S.C.V., W.D.B.; clinical studies, J.W.D.B., R.C., D.W., P.M.P., W.D.B.; statistical analysis, W.G.V., P.G., W.D.B.; and manuscript editing, J.W.D.B., W.G.V., S.C.V., A.D., D.W., P.M.P., P.G., W.D.B.

See Materials and Methods for pertinent disclosures.

Table 1

Patient Characteristics and Lung Function Parameters

				Spirometry				Bodyplethysmography			
Patient No.	Age (y)	Weight (kg)	Height (cm)	Forced Vital Capacity (L)	Forced Expiratory Volume (L)	Predicted Forced Expiratory Volume (%)	Predicted Tiffeneau Ratio (%)	Specific Airway Resistance (kPa·sec)	Residual Volume (L)	TLC (L)	FRC (L)
1	23	124.0	191	5.49	4.19	83.90	76.32	0.75	1.61	7.20	3.02
2	64	82.7	165	3.45	2.75	118.50	79.71	0.71	2.36	5.93	2.93
3	36	62.1	169	4.16	3.58	112.80	86.06	0.82	2.07	6.23	3.51
4	36	100.6	191	7.61	5.01	108.10	65.83	1.54	2.39	10.16	4.28
5	65	89.0	173	4.06	2.89	94.40	71.18	1.11	2.43	6.67	2.77
6	52	101.9	163	3.17	2.50	98.60	78.86	0.68	1.68	4.85	1.93
Overall*	46 ± 17	93.4 ±20.9	175 ±13	4.66 ±1.65	3.49 ±0.97	102.72 ±12.81	76.33 ±7.06	0.93 ±0.33	2.09 ±0.37	6.84 ±1.81	3.07 ±0.78

Note.—FRC = functional residual capacity, TLC = total lung capacity.

* Data are means ± standard deviations.

numeric flow simulations, including CT-based geometries and boundary conditions, with the outcome of SPECT/CT imaging. Special attention was given to the image-based patient-specific boundary conditions used in the numeric flow simulations.

Materials and Methods

Ethics and Disclosure

This study was approved by all relevant institutional review boards. All patients gave their signed informed consent. Novartis provided financial assistance for this study. Three authors (J.W.D.B., W.G.V., and S.C.V.) are consultants for FluidDA. One author (W.D.B.) is a director of and shareholder in FluidDA. Another author (A.D.) is employed by Novartis. Authors with no relation to the pharmaceutical industry had control over the inclusion of any data and information that might have presented a conflict of interest.

Patient Data

In this study, a total of six patients (mean age, 46 years; age range, 23–65 years) were enrolled. Three patients were men (mean age, 41 years; age range, 23–65 years), and three were women (mean age, 51 years; age range, 36–64 years). All patients had mild or moderate asthma, with an average forced expiratory volume of 102.7% ± 12.8 (standard deviation) and an average Tiffeneau ratio (forced expiratory volume divided by forced vital capacity) of 76.33% ± 7.06. The characteristics of these patients can be found in Table 1.

Thin-Section CT

All patients underwent two low-dose CT examinations: One was performed at functional residual capacity, which is the lung level attained after normal expiration. The other was performed at total lung capacity, which is the lung level attained after deep inhalation. The level of inspiration during CT was monitored with an in-house spirometry system that enables real-time monitoring of the breathing cycle. This ensured that the examinations were performed at the correct lung volume. A Lightspeed VCT scanner (GE Healthcare, Milwaukee, Wis) was used to obtain CT images.

The CT settings were as follows: tube voltage, 120 kV; tube current, 10–100 mAs; noise factor, 28; collimation, 0.625 mm; rotation time, 0.6 sec; and pitch factor, 1.375. A separate examination of the upper airway region was performed, in which the dose was reduced even further by reducing the tube voltage to 100 kV and the tube current to 20–30 mAs. The upper airway examination was performed during slow inhalation to prevent any patient-induced occlusion of the glottis. The total dose for the CT study was approximately 3–5 mSv. The acquisition time was approximately 2–8 seconds per scan.

Lobar and Airway Segmentation

CT data were subsequently read into a software package (Mimics; Materialise, Leuven, Belgium). This validated package (Food and Drug Administration, K073468; *Conformité Européenne* certificate, BE 05/1191.CE.01) enables segmentation of different anatomic regions by identifying and grouping voxels of the same anatomic structure. Consequently, these groups could be used to reconstruct the feature in three dimensions.

In this study, segmentation of all lung lobes and the respiratory tract was performed at FRC and TLC (Fig 1). Lung lobes were separated by identifying fissure lines on the CT images. Only oblique fissures in both lungs were included, since horizontal fissure in the right lung was often difficult to accurately determine with the SPECT/CT images because of the low-dose protocol. This resulted in definition of the volume of the left upper lobe, left lower lobe, right lower lobe, and a combination of the right upper and middle lobes. Values referring to the right lung consist of the sum of values of the right upper, middle, and lower lobes. Similarly, values referring to the left lung consist of the sum of values of the left upper and lower lobes.

Figure 1

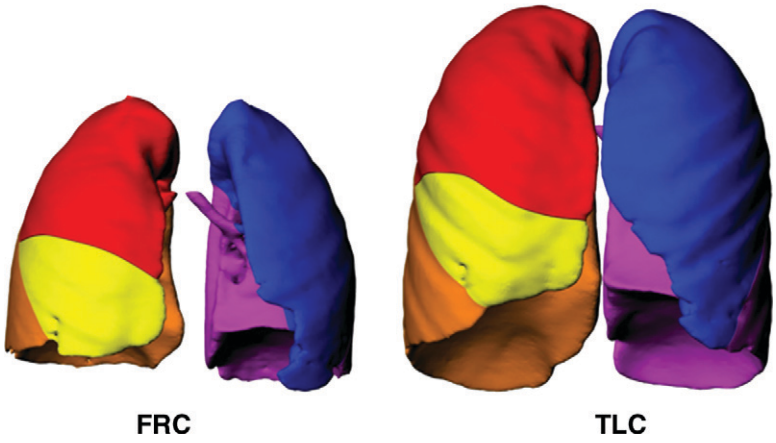

Figure 1: Segmentation of lungs and lobes after expiration at FRC and after deep inspiration at TLC to determine patient-specific lobar airflow distribution.

Figure 2

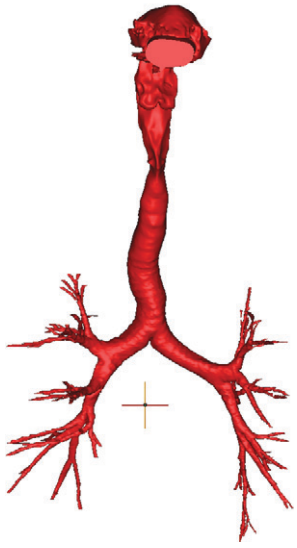

Figure 2: Three-dimensional reconstruction of the segmented airway structure down to the level of airways with a 1–2-mm diameter and including the extrathoracic airway structures.

By segmenting the lobes at FRC and TLC for each patient, the patient-specific airflow distribution could be established by assessing lobar volume expansion. This airflow distribution could be compared and validated with the lobar SPECT/CT tracer concentration and used as boundary conditions for CFD.

Besides the lung lobes, the respiratory tract was reconstructed down to the level of airways with a diameter of 1–2 mm (Fig 2). Beyond this point, the resolution of the image was not sufficient to enable us to distinguish intraluminal air from surrounding air in the alveolar space. The upper airway was reconstructed by using the same principles; thereafter, it was merged with the lower airway models by identifying a common landmark that was present on both the upper airway image and the lower airway image. The airway model at TLC was then prepared for CFD flow simulation by smoothing the airway wall by averaging the position of the surrounding vertices. This method is combined with Laplacian volume reduction compensation, where changes in vertex positions are used to determine volume changes and correct them. Subsequently, the outlets are cut perpendicular to the local centerline to ensure proper definition of outlet pressures. The outcome parameters obtained by using CT were a virtual model of the airway tree structure and a lobar expansion ratio. The latter represents the lobar distribution of the amount of inhaled air.

Flow Simulations and Particle Deposition

After segmentation and postprocessing, the airway model must be converted into a computational grid to solve the Navier-Stokes flow equations numerically. The computational tetrahedral grid was constructed with a commercial software package (TGrid 5.0.6; Ansys, Lebanon, NH). An initial surface-wrapping algorithm ensured a continuous airway wall; the subsequent refinement steps increase the cell density in the high-gradient regions, such as bends and curves.

Flow simulations were performed by using Fluent, version 6.3, software (Ansys). This software was used to solve the Reynolds-averaged Navier-Stokes equations, which are time-averaged equations of motion for fluid flow. The air in the lower airway was considered homogeneous, incompressible, and Newtonian. Turbulence was modeled with the low-Reynolds-number k-omega shear-stress transport model for transitional flows, as this model is well suited for particle deposition assessment at low velocities (29). The flow is considered steady so as to mimic the time-averaged inhalation of SPECT/CT tracer particles. The tracer particles were inhaled at a moderate inhalation rate, so an airflow rate of 30 L/min is specified at the model mouth (30). To obtain clinically relevant computational models, the geometry should be patient specific, and the boundary conditions must be defined in such a way that they reflect the patient-specific airflow distribution. To this end, the pressures that were imposed at the bronchioles were determined with an iterative routine, such that the airflow distribution in the computer model reflected the airflow distribution as derived from the expansion of the lung lobes from FRC to TLC. This ensures correct modeling of the resistance of the respiratory system where central and distal airway resistance is included via the patient-specific geometry, and peripheral resistance is accounted for by using the lobar expansion as boundary conditions (Fig 3).

Approximately 100000 discrete particles are injected in the numeric model on top of the flow by using a discrete phase method. This implies that the trajectories of discrete particles are determined by solving the force-mass balance on each individual particle. The boundary condition on the airway is set such that whenever a particle hits the wall it is trapped there. This makes it possible to determine local deposition

Figure 3

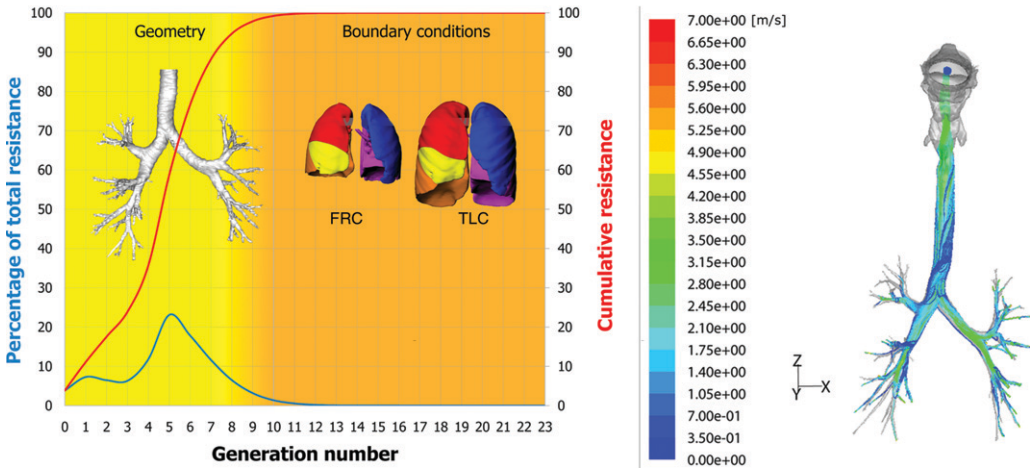

Figure 3: Left: Patient-specific boundary conditions for CFD simulations based on lobar expansion to account for resistance induced by peripheral airways with a diameter of less than 1 mm. Right: Calculated particle paths with CFD colored by particle velocity (in meters per second).

patterns. Particles injected in the CFD model have the same characteristics as the inhaled SPECT/CT tracer (SmartVent). The diameter of the particles in the tracer was reported to be 1.32 μm. The particles were injected centrally at the mouth. The sum of particulate fraction leaving the model toward the selected lobes and the deposited particles in the individual airways was considered a CFD output parameter. CFD simulations were run in parallel on four computers. Converged flow fields were obtained in approximately 12–16 hours.

SPECT/CT

Patients underwent SPECT/CT within 24 hours after CT. For ventilation SPECT/CT, a radioaerosol delivery system (SmartVent) was used with ^{99m}Tc pentetic acid. The administered activity of ^{99m}Tc pentetic acid was 500 MBq in the nebulizer, from which the patient received approximately 50 MBq in the lungs. The aerosol was administered through a mouth piece, with the nose occluded and the patient performing slow tidal breathing. SPECT/CT images were acquired by using a dual-head SPECT/CT camera with 180° geometry (Symbia T6; Siemens Medical Solutions, Erlangen, Germany). A total of 64 projections were obtained (32 projections were acquired with each head, 180° rotation, 15 seconds for each projection, 128 × 128 matrix, 1.0 zoom factor). After acquisition of SPECT/CT images, the patient remained immobilized in the supine position, and low-dose CT was performed (tube voltage, 130 kV; effective tube current, 70 mAs; collimation, 6 × 2.0 mm; rotation time, 0.6 sec; pitch, 1.4) after normal inspiration. Total acquisition time was about 15 minutes. The radiation dose for SPECT/CT was approximately 4 mSv.

Standard Siemens Medical Solutions software was used to process the SPECT/CT images. Iterative fast low-angle shot three-dimensional reconstruction (four subsets; eight iterations; Gaussian filter, 8.4) was used to obtain frontal, sagittal, and transverse projections, as well as to rotate three-dimensional images.

Lobar Tracer Concentrations

The SPECT/CT images were read into a software package (Osirix, version 3.5.1; OsiriX Imaging Software, Geneva, Switzerland). SPECT/CT tracer and CT images were re-registered and subsequently fused at corresponding locations. The contours of the lung lobes were marked with the region of interest method. Identification of the bounding contours was based on the CT images, which enabled determination of lobar tracer concentration by transferring the region of interest contours onto the SPECT/CT images. The lobe definition technique was the same as that used with the CT images (right upper and right middle lobes, right lower lobe, left upper lobe, left lower lobe). Thus, the outcome parameter of SPECT/CT was the lobar tracer distribution, which is a measure of the distribution of inhaled air.

Results

The CT results showed that in all patients, the lower lobes receive a larger percentage of inhaled air than do the upper lobes. On average, the right and left lower lobes received 30.1% ± 2.8 and 30.8% ± 2.8 of the inhaled air, respectively, while the right upper and right middle lobes and the left upper lobe received 21.2% ± 2.3 and 18.0% ± 2.4 of the inhaled air, respectively (Table 2).

Heterogeneity of Lobar Distribution of Inhaled Air

Lobar distribution of inhaled air was inhomogeneous in the studied population. The amount of air toward the different lung lobes varied from patient to patient. The maximum difference was 10.4% for SPECT/CT data in the left lower lobe, 7.8% for CT data in the right lower lobe; and 11.2% for CFD data in the right lower lobe. An overview of the

Table 2

Lobar Distribution of Inhaled Air for SPECT/CT, CT, and CFD

	Right Upper and Right Middle Lobes			Right Lower Lobe			Left Upper Lobe			Left Lower Lobe		
Patient No.	SPECT/CT	CT	CFD	SPECT/CT	CT	CFD	SPECT/CT	CT	CFD	SPECT/CT	CT	CFD
1	26.1	22.9	24.6	27.4	26.6	27.2	18.0	17.4	17.5	28.5	33.1	30.6
2	25.3	18.2	21.1	31.8	34.4	36.4	16.6	14.9	13.3	26.2	32.5	29.2
3	17.3	18.9	18.1	33.9	31.1	28.3	14.5	17.0	21.5	34.4	33.1	32.0
4	22.3	22.6	22.8	26.7	28.6	27.9	21.4	19.4	20.0	29.5	29.4	29.4
5	24.9	23.8	24.9	28.7	28.2	25.2	22.4	22.0	22.0	24.0	26.0	27.9
6	23.2	20.6	22.3	32.3	31.7	31.9	15.0	17.3	16.7	29.5	30.4	29.1
Overall*	23.2 ± 3.2	21.2 ± 2.3	22.3 ± 2.5	30.1 ± 2.9	30.1 ± 2.8	29.5 ± 4.0	18.0 ± 3.3	18.0 ± 2.4	18.5 ± 3.3	28.7 ± 3.5	30.8 ± 2.8	29.7 ± 1.4

Note.—Data are percentages of inhaled air.

* Data are means ± standard deviations.

differences in lobar distribution for all methods can be found in Table 3.

When considering the intrapatient tracer deposition patterns, it was observed that in patients 1 and 4, an inhomogeneous distribution of the tracer was present, with formation of local hot spots (Fig E1 [online]). In patient 1, these local hot spots were positioned throughout the left and right lungs; however, in patient 4, the hot spots were localized at the right and left main bronchi. Although the hot spots could be clearly distinguished, the spatial resolution of the SPECT/CT method is not sufficient to correlate aerosol deposition with local airway geometry. The other patients had a more homogeneous (no distinct hot spots) tracer distribution, with a clear tendency for the tracer to deposit in the lower lobes.

In Figure 4, segmentation results at FRC and TLC, CFD-based particle deposition, and SPECT/CT data are compared, with the focus on the right upper lobe bronchi of patient 4. From the segmented images, one can see that parts of the airways are closed at FRC. Lumen narrowing remains at TLC, even while all the airways are open. Consequently, these airway dynamics (flow through a narrow region) cause a local build-up of particles, resulting in a hot spot that can be detected with both SPECT/CT and CFD.

Flow Simulation and CT-based Lobar Expansion versus SPECT/CT Tracer Concentration

The results showed good agreement between the airflow distribution as determined by using CT-based lobar expansion and through quantification of SPECT/CT tracer concentration (Figs 5, E2 [online]). The average difference between the two methods for all lobes was less than 3% (Fig 6). For all individual patients, the maximum difference was less than 5%. with the exception of patient 2, in whom a maximum difference of 7.2% was found for the right upper and right middle lobes. Also, the airflow distribution determined by using CFD and particle tracking compared well with the SPECT/CT data (Figs 5, E2 [online]). Again, the mean difference was less than 3% (Fig 6), and the maximum difference was less than 5%, with the exception of patient 3, in whom the maximum difference was 7%.

When averaging the results of all patients, the difference between all methods becomes small, with a maximum difference of 2.0%, 0.7%, 0.5%, and 2.1% for the right upper and right middle lobes, right lower lobe, left upper lobe, and left lower lobe, respectively.

Table 3

Range of Inhaled Air toward the Indicated Lobes

Modality	Right Upper and Right Middle Lobes	Right Lower Lobe	Left Upper Lobe	Left Lower Lobe
SPECT/CT	17.3–26.1	26.7–33.9	14.5–22.4	24.0–34.4
CT	18.2–23.8	26.6–34.4	14.9–22.0	26.0–33.1
CFD	18.1–24.9	25.2–36.4	13.3–22.0	27.9–32.0

Note.—Data are percentages of inhaled air.

Discussion

The aim of this study was to compare the intrathoracic flow distribution between CFD simulations based on segmented CT images (hereafter, CT/CFD) and a SPECT/CT method with inhaled aerosols. SPECT/CT was selected, as this is presently one of the tests that yields the most accurate three-dimensional distribution of inhaled tracers, with a field of view that covers the entire thorax. The more widely used CT technique and the CFD approach could yield similar information when SPECT/CT is not available. We conducted this comparison study to ensure the accuracy of the latter approach.

The results showed that even in this population of patients with mild asthma, heterogeneous behavior is observed both in the interpatient differences between the lobar distribution of inhaled air and in local deposition behavior (hot spot formation) of the SPECT /CT tracer. Thus, it was interesting to see whether this inhomogeneous behavior resulted in

large differences between the different techniques. The results demonstrated good agreement between all methods, with limited differences between the lobar air distributions obtained with the different methods, despite the inherent patient-specific nature of this parameter. This indicates that CFD, when based on CT data, can be used to accurately describe regional lobar distribution. In addition, the formation of hot spots could be qualitatively explained on the basis of imaging and CFD data by assessing airway changes from FRC to TLC.

Previously, Campana et al (31) and Venegas et al (32) studied the heterogeneity of ventilation in patients with asthma by using hyperpolarized helium. The present study also demonstrates that similar behavior is present in this set of patients with mild to moderate asthma when SPECT/CT and CT/CFD are used. Thus, the CT/CFD technique could complement the helium method to permit deeper insight into the pathophysiology of this disease and enable us to study the effect of inhomogeneous ventilation on patient health.

For the first time, patient-specific CFD flow and particle simulations have been compared with other state-of-the-art functional imaging tools, such as SPECT/CT, in a relevant patient population. The good agreement indicates that when one uses appropriate boundary conditions, results of numerical simulations correspond to data obtained in vivo. The required boundary conditions could be deduced from the images by assessing the lobar expansion from FRC to TLC, since this CT-based lobar expansion provides a good representation of SPECT/CT tracer distribution.

Although SPECT/CT images yield a good visual representation of the patient-specific lung ventilation, the method itself has some downsides, making it less optimal for use as a standard test in clinical routine. For instance, SPECT/CT examination time is substantially longer than CT examination time; therefore, fewer patients can be analyzed in the same time frame. The need to inhale a tracer makes SPECT/CT slightly more invasive than CT and requires increased patient cooperation. In addition

Figure 4

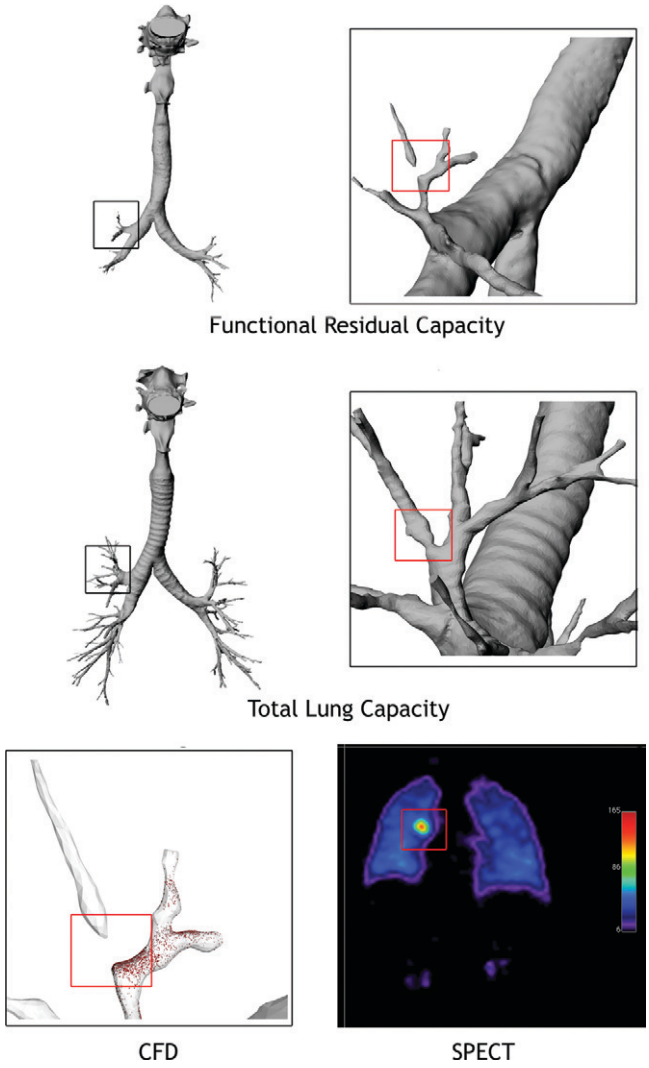

Figure 4: Top and middle: Three-dimensional reconstructions of the airway models of patient 4 at FRC (top) and TLC (middle) show central airway occlusion at FRC. Bottom: Comparison of hot spot formation determined with CFD and SPECT/CT. In all images, boxes indicate an airway that is occluded at FRC. The same airway reopens at TLC; however, narrowing remains, as in the middle image. Particles will form a hot spot at this location, as can be seen on the CFD and SPECT/CT images.

SPECT/CT units are not as widely available as CT units. The good comparison between the methods implies that CT and CFD could complement SPECT/CT and yield additional valuable outcome parameters in future studies. It also indicates that CFD and CT enable one to predict the distribution of inhaled air and particles in the lung. The question of regional lung ventilations becomes highly relevant in patients with heterogeneous or regional lung disease, as is the case in patients with acute respiratory distress syndrome (33), chronic obstructive pulmonary disease (34), and severe asthma (35). Our study demonstrated that by analyzing the lobar expansion from FRC to TLC the regional lung ventilation could also be assessed. By repeating the analyses before and after an intervention or during the course of a pharmacologic treatment, it becomes

Figure 5

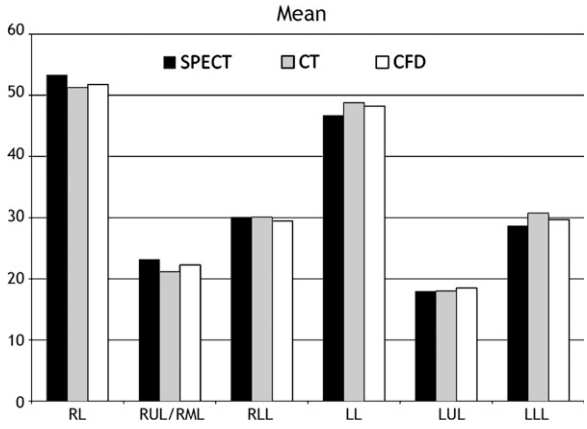

Figure 5: Graph shows airflow distribution (measured as percentage of inhaled air), as determined with SPECT/CT, CT, and CFD, indicating limited differences between all methods. *RL* = right lung, *RUL/RML* = right upper and right middle lobes, *RLL* = right lower lobe, *LL* = left lung, *LUL* = left upper lobe, *LLL* = left lower lobe.

Figure 6

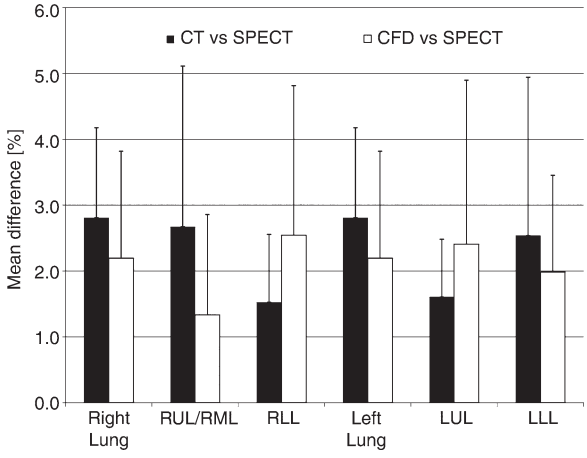

Figure 6: Graph shows mean difference (bar) and standard deviation (vertical line) in airflow between CT and SPECT/CT and between CFD and SPECT/CT. *RL* = right lung, *RUL/RML* = right upper and right middle lobes, *RLL* = right lower lobe, *LL* = left lung, *LUL* = left upper lobe, *LLL* = left lower lobe.

possible to detect changes in airway morphology and diameter and to assess airway recruitment and subsequent local changes in lung ventilation. On the other hand, CFD and particle deposition studies can be used in preclinical and clinical development of inhaled compounds and inhaler devices, as this method enables detection of aerosol behavior and topical deposition patterns, as the comparison with the SPECT/CT outcomes in this study indicates. The advantage is that for an inhalation device or a formulation, the drug distribution and deposition in the lung can be predicted on the basis of patient-specific data and boundary conditions that have been acquired with CT once, without the need for repeated patient involvement. The models can also be used in preclinical drug development to predict commonalities and differences between preclinical in vivo experiments and patient studies in terms of lung ventilation and drug disposition.

This study had a number of limitations. A qualitative comparison between local particle deposition concentrations at airway level is difficult because of the difference in resolution between SPECT/CT data and CT/CFD data. In future studies, combined positron emission tomography (PET)/CT could be considered, as the spatial resolution of this technique could be higher. It must be stated that PET aerosol studies are challenging to perform and the improvement in spatial resolution is not guaranteed. Although computational clinical research appears to be a promising field, additional developments have to be undertaken prior to structural implementation. At present, the airway segmentation is still relatively time consuming (2–3 hours), especially the manual interventions at the small airway level. Future software segmentation packages must be tailored toward optimization of this topic.

In conclusion, this study demonstrated the patient-specific character of lobar distribution of inhaled air with three methods (SPECT/CT, CT, and CFD). There was a good correlation between the methods, indicating that results from CFD computations in combination with patient-specific boundary conditions coming from CT yield results that correspond well with in vivo measurements, such as SPECT/CT and CT. On the basis of these findings, it becomes feasible to use functional imaging for analysis and optimization of drug delivery and respiratory devices.

References

1. Boiselle PM. Imaging of the large airways. Clin Chest Med 2008;29(1):181–193, vii.
2. Coxson HO, Rogers RM. New concepts in the radiological assessment of COPD. Semin Respir Crit Care Med 2005;26(2):211–220.
3. Litmanovich D, Boiselle PM, Bankier AA. CT of pulmonary emphysema: current status, challenges, and future directions. Eur Radiol 2009;19(3):537–551.
4. Matsuoka S, Kurihara Y, Yagihashi K, Hoshino M, Nakajima Y. Airway dimensions at inspiratory and expiratory multisection CT in chronic obstructive pulmonary disease: correlation with airflow limitation. Radiology 2008;248(3):1042–1049.
5. Corren J. Small airways disease in asthma. Curr Allergy Asthma Rep 2008;8(6):533–539.
6. de Blic J, Scheinmann P. The use of imaging techniques for assessing severe childhood asthma. J Allergy Clin Immunol 2007;119(4):808–810.
7. Nakano Y, Van Tho N, Yamada H, Osawa M, Nagao T. Radiological approach to asthma and COPD: the role of computed tomography. Allergol Int 2009;58(3):323–331.
8. Brody AS. Scoring systems for CT in cystic fibrosis: who cares? Radiology 2004;231(2):296–298.
9. Loeve M, Lequin MH, de Bruijne M, et al. Cystic fibrosis: are volumetric ultra-low-dose expiratory CT scans sufficient for monitoring related lung disease? Radiology 2009;253(1):223–229.

10. Saavedra MT, Lynch DA. Emerging roles for CT imaging in cystic fibrosis. Radiology 2009;252(2):327–329.

11. De Backer JW, Vos WG, Devolder A, et al. Computational fluid dynamics can detect changes in airway resistance in asthmatics after acute bronchodilation. J Biomech 2008; 41(1):106–113.

12. De Backer JW, Vos WG, Verhulst SL, De Backer W. Novel imaging techniques using computer methods for the evaluation of the upper airway in patients with sleep-disordered breathing: a comprehensive review. Sleep Med Rev 2008;12(6):437–447.

13. Lin CL, Tawhai M, McLennan G, Hoffman E. Computational fluid dynamics. IEEE Eng Med Biol Mag 2009;28(3):25–33.

14. Anderson J. Computational fluid dynamics. New York, NY: McGraw-Hill, 2001.

15. Nowak N, Kakade PP, Annapragada AV. Computational fluid dynamics simulation of airflow and aerosol deposition in human lungs. Ann Biomed Eng 2003;31(4):374–390.

16. Isaacs KK, Schlesinger RB, Martonen TB. Three-dimensional computational fluid dynamics simulations of particle deposition in the tracheobronchial tree. J Aerosol Med 2006;19(3):344–352.

17. Longest PW, Vinchurkar S. Effects of mesh style and grid convergence on particle deposition in bifurcating airway models with comparisons to experimental data. Med Eng Phys 2007;29(3):350–366.

18. Luo HY, Liu Y, Yang XL. Particle deposition in obstructed airways. J Biomech 2007; 40(14):3096–3104.

19. Brook BS, Murphy CM, Breen D, Miles AW, Tilley DG, Wilson AJ. Quantification of lung injury using ventilation and perfusion distributions obtained from gamma scintigraphy. Physiol Meas 2007;28(12): 1451–1464.

20. Newman SP, Pitcairn GR, Hirst PH. A brief history of gamma scintigraphy. J Aerosol Med 2001;14(2):139–145.

21. Fleming JS, Epps BP, Conway JH, Martonen TB. Comparison of SPECT aerosol deposition data with a human respiratory tract model. J Aerosol Med 2006;19(3): 268–278.

22. Suga K, Kawakami Y, Iwanaga H, Tokuda O, Matsunaga N. Automated breath-hold perfusion SPECT/CT fusion images of the lungs. AJR Am J Roentgenol 2007;189(2): 455–463.

23. Suga K, Yasuhiko K, Iwanaga H, Tokuda O, Matsunaga N. Functional mechanism of lung mosaic CT attenuation: assessment with deep-inspiration breath-hold perfusion SPECT-CT fusion imaging and non-breath-hold Technegas SPECT. Acta Radiol 2009;50(1): 34–41.

24. Nagao M, Murase K, Ichiki T, Sakai S, Yasuhara Y, Ikezoe J. Quantitative analysis of technegas SPECT: evaluation of regional severity of emphysema. J Nucl Med 2000;41(4):590–595.

25. Xu J, Moonen M, Johansson A, Gustafsson A, Bake B. Quantitative analysis of inhomogeneity in ventilation SPET. Eur J Nucl Med 2001;28(12):1795–1800.

26. de Rochefort L, Vial L, Fodil R, et al. In vitro validation of computational fluid dynamic simulation in human proximal airways with hyperpolarized 3He magnetic resonance phase-contrast velocimetry. J Appl Physiol 2007;102(5):2012–2023.

27. Mylavarapu G, Murugappan S, Mihaescu M, Kalra M, Khosla S, Gutmark E. Validation of computational fluid dynamics methodology used for human upper airway flow simulations. J Biomech 2009;42(10):1553–1559.

28. De Backer JW, Vos WG, Gorlé CD, et al. Flow analyses in the lower airways: patient-specific model and boundary conditions. Med Eng Phys 2008;30(7):872–879.

29. Wilcox DC. Turbulence modeling for CFD. 2nd ed. La Cañada, Calif: DCW Industries, 1998.

30. Usmani OS, Biddiscombe MF, Barnes PJ. Regional lung deposition and bronchodilator response as a function of beta2-agonist particle size. Am J Respir Crit Care Med 2005;172(12):1497–1504.

31. Campana L, Kenyon J, Zhalehdoust-Sani S, et al. Probing airway conditions governing ventilation defects in asthma via hyperpolarized MRI image functional modeling. J Appl Physiol 2009;106(4):1293–1300.

32. Venegas JG, Winkler T, Musch G, et al. Self-organized patchiness in asthma as a prelude to catastrophic shifts. Nature 2005; 434(7034):777–782.

33. Gattinoni L, Caironi P, Cressoni M, et al. Lung recruitment in patients with the acute respiratory distress syndrome. N Engl J Med 2006;354(17):1775–1786.

34. Verbanck S, Schuermans D, Vincken W. Small airways ventilation heterogeneity and hyperinflation in COPD: response to tiotropium bromide. Int J Chron Obstruct Pulmon Dis 2007;2(4):625–634.

35. Bayat S, Porra L, Suhonen H, et al. Imaging of lung function using synchrotron radiation computed tomography: what's new? Eur J Radiol 2008;68(3 suppl):S78–S83.